Excitation of the 4.3-μm bands of CO_2 by low-energy electrons*

B. R. Bulos† and A. V. Phelps‡

Joint Institute for Laboratory Astrophysics, National Bureau of Standards and University of Colorado, Boulder, Colorado 80309

(Received 22 March 1976)

Rate coefficients for the excitation of the 4.3-μm bands of CO_2 by low-energy electrons in CO_2 have been measured using a drift-tube technique. The CO_2 density [$(1.5 \text{ to } 7) \times 10^{17}$ molecules/cm^3] was chosen to maximize the radiation reaching the detector. Line-by-line transmission calculations were used to take into account the absorption of 4.3-μm radiation. A small fraction of the approximately 10^{-8} W of the 4.3-μm radiation produced by the approximately 10^{-7}-A electron current was incident on an InSb photovoltaic detector. The detector calibration and absorption calculations were checked by measuring the readily calculated excitation coefficients for vibrational excitation of N_2 containing a small concentration of CO_2. For pure CO_2 the number of molecules capable of emitting 4.3-μm radiation produced per cm of electron drift and per CO_2 molecule varied from 10^{-17} cm^{-2} at $E/N = 6 \times 10^{-17}$ Vcm^2 to 5.4×10^{-16} cm^{-2} at $E/N = 4 \times 10^{-16}$ Vcm^2. Here E is the electric field and N is total gas density. The excitation coefficients at lower E/N are much larger than estimated previously. A set of vibrational excitation cross sections is obtained for CO_2 which is consistent with the excitation coefficient data and with most of the published electron-beam data.

I. INTRODUCTION

This paper reports direct measurements of the rate coefficients for the excitation of the 4.3-μm bands of the CO_2 molecule by low-energy electrons. Because of the long radiative lifetime (2.2 msec) of the vibrational levels responsible for this radiation, primarily from the 001 level, and because of the low electron energies of interest, we have made the measurements using an electron drift tube[1] operating at gas densities such as to maximize the intensity of the emitted 4.3-μm radiation.

Drift tubes have been used previously to measure rate coefficients for the excitation of visible and near-ultraviolet radiation from states with short radiative lifetimes in hydrogen[2,3] and nitrogen.[3] The advantages of excitation coefficient measurements using the drift tube relative to measurements in electrical discharges[4,5] are that low values of the ratio of the electrical field to the gas density, E/N, can be obtained and that a properly operated drift tube is free from space-charge-related effects, such as the cathode sheath and striations.[6] The advantages of the drift tube relative to low-energy electron beam measurements are that the use of moderate gas densities maximizes the radiated energy and that the mean electron energy is readily varied from well below the excitation threshold (0.291 eV) to well above threshold. The primary disadvantage of the drift-tube technique is that the extraction of details regarding the energy dependence of the excitation cross section from the measured rate coefficients is hampered by the inherently low percentage energy resolution which characterizes the steady-state electron energy distributions.[7]

Interest in the excitation of the vibrational levels of CO_2 by electrons has increased in recent years, particularly because of the development of CO_2 lasers[8] and because of the role of energy exchange between electrons and CO_2 in planetary atmospheres.[9] This interest has led to measurements of cross sections for the inelastic scattering of electrons,[10-12] determinations of rates of excitation in discharges from analyses of laser gain,[13-15] theoretical calculations of cross sections for optically allowed and forbidden traisitions,[16] and attempts to derive sets of cross sections which are consistent with theory and electron-beam studies[17] and with measured electron transport coefficients.[18,19] The available cross-section data have been used in the prediction of excitation rate coefficients, electron mobilities, etc.[19-21] for gas mixtures appropriate to electrical discharge and electron-beam sustained lasers.

The theoretical basis of the experiment is discussed in Sec. II. Section III contains a description of the experimental apparatus and procedures. The results of the experiment are presented and discussed in Sec. IV. A set of vibrational excitation cross sections consistent with the excitation coefficient data, electron transport data, and with electron-beam-experiment data is given in Sec. V.

II. THEORY OF EXPERIMENT

A. Pure CO_2

The vibrational levels of the lowest electronic state of the CO_2 molecule of importance in this experiment are shown in Fig. 1. The fundamental modes are the ν_1 or symmetric stretch mode, the

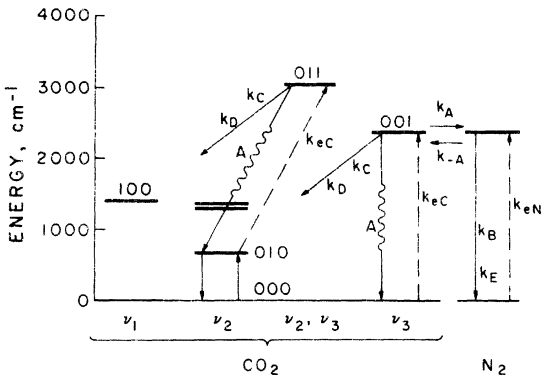

FIG. 1. Energy levels of the lower vibrational states of CO_2 and N_2 showing radiative and collisional transitions of importance in the experiments discussed in this paper.

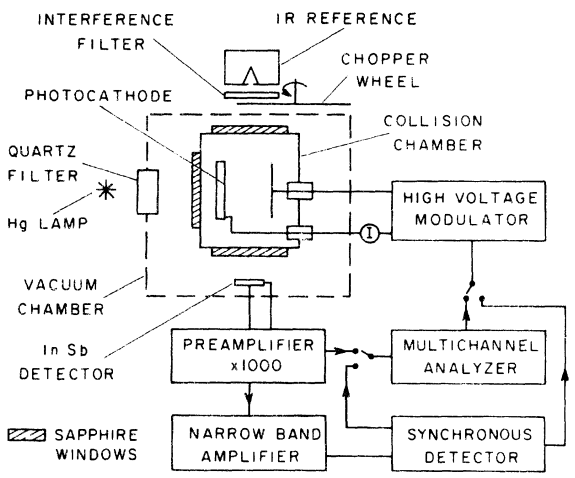

FIG. 2. Schematic of experiment with detail of drift-tube collision chamber.

ν_2 or bending mode, and the ν_3 or asymmetric stretch mode. In addition, there are levels which can be regarded as a mixture of the fundamental modes, e.g., the 011 level. Since the response of our detector decreases rapidly[22] for wave lengths larger than 5.5 μm, we detect only transitions involving a change of one or more quantum numbers in the ν_3 mode or changes involving more than one quantum number in the ν_1 and ν_2 modes. Furthermore, the low degree of excitation[23] and the relatively large number of collisions (greater than 1000) within the time resolution of our experiment insure a Boltzmann population[24,25] of vibrationally excited molecules at a vibrational temperature slightly above the gas temperature, e.g., $\Delta T_V = 0.3$ K. This combination of factors results in the detectable radiant energy being emitted primarily in the 001 → 000 band near 2349 cm^{-1} and in the 011 → 010 band near 2336 cm^{-1}. Since the relative populations of the 001 and 011 levels rapidly reach equilibrium by collisions,[25] we will treat them as one level in the discussion of the rate equations.

A schematic diagram of the experimental arrangement is shown in Fig. 2. The excitation of the CO_2 takes place in a collision chamber filled with CO_2 at densities between 1×10^{16} and 20×10^{16} molecules/cm^3 as the result of a current of electrons moving between the photocathode and the anode under the influence of a uniform electric field. A portion of the radiation emitted by the excited molecules passes through the gas to a window and its intensity is measured by an InSb photovoltaic detector. In order to discriminate against background radiation emitted by the walls of the collision chamber and against scattered radiation from the Hg lamp used to illuminate the photocathode, the electric field and thereby the electron current are 100% modulated at some convenient frequency, e.g., ~295 Hz. The modulated signal from the InSb detector is amplified and either enters the multichannel analyzer, where it is recorded as a transient waveform for later analysis, or enters a narrow-band amplifier and lock-in detector.

The behavior of the photoelectrons which enter and drift through a gas under the action of the uniform applied electric field has been discussed in a number of reviews.[1,7] In a gas with large inelastic collision cross sections, such as[18] CO_2, the electrons rapidly reach a steady-state distribution of energies in which the rate of energy gain from the electric field E is balanced by the rate of energy-loss collisions with the gas of density N. At the low percentage ionization ($< 10^{-10}$) and low degree of excitation characteristic of the present experiments this balance results in an electron energy distribution which generally shows significant departures from a Maxwellian,[18-20] but which is a unique function of the E/N ratio and the gas temperature. The rate coefficients k_J for various collision processes, such as excitation, are found by averaging the appropriate cross section $\sigma_J(\epsilon)$ over the normalized energy distribution $\epsilon^{1/2}f(\epsilon)$, i.e.,

$$k_J = \left(\frac{2}{m}\right)^{1/2} \int_{\epsilon_J}^{\infty} \epsilon \sigma_J(\epsilon) f(\epsilon)\, d\epsilon \,. \tag{1}$$

Here ϵ is the electron energy, ϵ_J is the threshold for the collision process, and m is the electron mass. In some cases it is convenient to express the rate coefficients in the terms of the number of events per unit distance of electron drift in the field direction rather than per unit time as in Eq. (1). These generalized Townsend coefficients[1] are

defined by

$$\alpha_J = k_J N/w, \tag{2}$$

where w is the electron drift velocity.

The differential equation describing the time dependence of the excited CO_2 density n_C is

$$\frac{\partial n_C}{\partial t} = -gA n_C - k_c N n_C + D\nabla^2 n_C + k_{eC} N n_e, \tag{3}$$

where g is the Holstein imprisonment factor[26] which accounts for absorption of the 4.3-μm radiation by CO_2, A is the radiative transition probability,[27] k_c is the rate coefficient[28, 29] for deexcitation of the ν_3 mode in collisions with ground-state molecules of density N, D is the excited molecule diffusion coefficient,[29] and k_{eC} is the rate coefficient for excitation[19, 20] of the CO_2 to the 001 and 011 levels by electrons of density n_e. Deexcitation by electrons can be neglected at the low electron densities ($<10^6$ cm^{-3}) of these experiments. Radiative transitions from the 001 level to the 100 and 02^{0}0 levels can also be neglected. We can approximate the effect of the diffusion term by using solutions of Eq. (3) appropriate to the fundamental diffusion mode,[30] i.e., replace $D\nabla^2 n_C$ by $-Dn_C/\Lambda^2$, where $\Lambda^{-2} = (\pi/L)^2 + (2.4R)^2$ is the diffusion length and R and L are the radius and length of the experimental tube. Equation (3) then becomes

$$\frac{dn_C}{dt} = -\gamma n_C + k_{eC} N n_e, \tag{4}$$

where the decay constant γ is given by

$$\gamma = gA + k_c N + D/\Lambda^2. \tag{5}$$

The use of Holstein's g factor is also the result of the use of an approximate solution to the complete integrodifferential equation.[30] Our experimental conditions are such that $gA \ll k_c N + D/\Lambda^2$ for all gas densities used, i.e., most of the excited molecules are destroyed before radiative transport can change their spatial distribution.

Since (a) the distance through which the electrons move before reaching the steady-state energy distribution is small,[1, 18] (b) the transit time of the electrons[1, 18] across the drift tube ($\sim 1\,\mu$sec) is short compared to the time resolution of our apparatus, (c) the illumination of the photocathode is independent of time, and (d) the E/N values are low enough so that electron attachment and ionization can be neglected,[18] we can assume that the electron density in Eqs. (3) and (5) is independent of time and position during the period of constant applied field. During the period of zero applied field the few electrons remaining in the drift tube rapidly ($\sim 0.1\,\mu$sec) cool[18] to the gas temperature, so that for the purposes of Eqs. (3) and (5) the density of electrons capable of producing excited molecules is zero. It is convenient to express the electron density in terms of the electron current density j using the $j = ewn_e$. Under these conditions the solution for the excited molecule density with negligible initial n_C is

$$n_C = (k_{eC} N j/ew\gamma)(1 - e^{-\gamma t}) = (\alpha_C j/e\gamma)(1 - e^{-\gamma t}), \tag{6}$$

where j is the current density during the period of application of the field beginning at $t = 0$. Following a sufficiently long voltage pulse,

$$n_C = (\alpha_C j/e\gamma) e^{-\gamma t'}, \tag{7}$$

where t' is measured from the time of removal of the field. Note that for short times, i.e., $\gamma t \ll 1$, Eq. (6) becomes

$$n_C = \alpha_C j t/e. \tag{8}$$

This means that if one measures the initial rate of rise of the excited atom density n_C/t or the corresponding rate of rise of radiated energy one does not need to measure the decay constant γ. This relation also follows from Eqs. (3) and (4), for small n_C.

An important simplification of Eqs. (6) and (7) occurs at the high gas densities at which our excitation coefficients were determined (see Appendix A). In this limit $D/\Lambda^2 \ll k_C N$, so that diffusion losses can be neglected. The magnitude factor in Eqs. (6) and (7) then becomes

$$n_C(\max) \equiv \alpha_C j/e\gamma = (\alpha_C/N) j/e k_c, \tag{9}$$

so that the excited molecule density per unit current density is independent of the CO_2 density at fixed E/N and gas temperature. This feature places an upper limit on the density of excited molecules which can be produced in a space-charge-free drift tube for a given gas. It also means that for densities of CO_2 such that diffusion loss is negligible the addition of an atomic gas can increase the excited molecule density only through a possible increase in α_C. On the other hand, foreign gases can reduce the excited molecule density through an increase in quenching. The effect of adding molecular gases with nearly resonant energy levels, such as N_2, will be discussed in Sec. II B.

The magnitude of the signal, S, developed by the detector as the result of the radiation emitted by the excited molecules in the drift tube is calculated from the relation

$$S = f_d D(\nu_0) A h\nu_0 \int_V \frac{\Delta\Omega}{4\pi} \mathcal{T}(\rho) n_C \, dV, \tag{10}$$

where f_d is the fractional transmission of the windows between the gas of the cell and the detector, $D(\nu_0)$ is the responsitivity of the detector at the

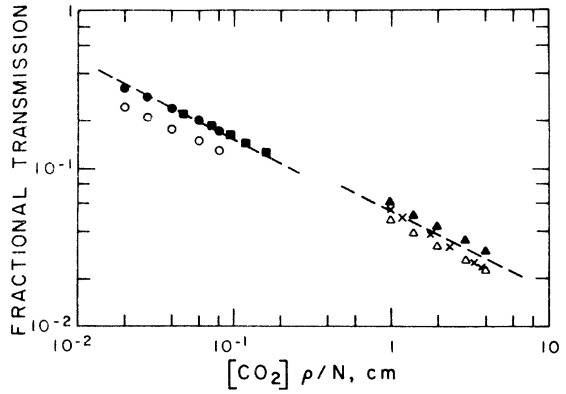

FIG. 3. Calculated fractional transmission of CO_2 4.3-μm radiation through CO_2 and CO_2-N_2 mixtures. Contributions to the emission and absorption by the 001-000 bands of $^{12}CO_2$ and $^{13}CO_2$ and the 011-010 band of $^{12}CO_2$ are included as described in Appendix B. The symbols and associated values of percent CO_2, temperature, and total gas density are ●: 2%CO_2, 300 K, 1.6×10^{18} cm^{-3}; ■: 4%CO_2, 300 K, 1.6×10^{18} cm^{-3}; ○: 2%CO_2, 204K, 2.4×10^{18} cm^{-3}; ▲: 100%CO_2, 300 K, 3.2×10^{17} cm^{-3}; △: 100%CO_2, 205K, 4.7×10^{16} cm^{-3}; and ×: 100%CO_2, 300K, 1.6×10^{18} cm^{-3}. The dashed curves give the predictions of the approximate formula of Appendix B.

frequency ν_0 of the origin of the 4.3μm transition, $\mathcal{T}(\rho)$ is the fraction of the 4.3-μm band which traverses the distance ρ from the point of production to the window nearest the detector, $\Delta\Omega$ is the solid angle subtended by the detector from the volume element and h is Plank's constant.

The calculation of the transmission factor $\mathcal{T}$ is very involved because of the large number of rotational transitions in the 4.3-μm band, and is summarized in Appendix B. The results of this calculation are given in Fig. 3. The transmission factor $\mathcal{T}$ decreases approximately as the square root of the distance ρ through which the radiation passes. At a fixed temperature and intermediate CO_2 densities the transmission factor is independent of the CO_2 density. Both of these characteristics are as expected for isolated, self-broadened, and Lorentzian-shaped lines.[26] The approximately 30% increase in $\mathcal{T}$ when the temperature is raised from 204 to 300 K is almost entirely due to the increased contribution of the 011→010 transition, which is thermally excited and which is relatively weakly absorbed. The decrease in $\mathcal{T}$ for pure CO_2 at 300 K when the CO_2 density is increased from 3.2×10^{17} to 1.6×10^{18} cm^{-3} is caused by the overlapping of neighboring lines in the CO_2 absorption spectrum (see Appendix B). As expected, this effect becomes more pronounced as the distance ρ is increased.

The magnitude of the signal developed by the detector when illuminated by the blackbody in the absence of CO_2 in the cell is given by

$$S_b = f_d f_b A_b \Delta\Omega_b D(\nu_i) \int_0^\infty f_i(\nu) B(\nu)\, d\nu \,, \tag{11}$$

where f_b is the fractional transmission of the windows near the blackbody, A_b is the area of the limiting aperture between the blackbody and the detector, $\Delta\Omega_b$ is the solid angle of the detector as seen from the limiting aperture, $f_i(\nu)$ is the fractional transmission of the interference filter between the blackbody and the collision chamber, $B(\nu)$ is the intensity of the radiation emitted by the blackbody per unit area at the frequency ν, and $D(\nu_i)$ is the sensitivity of the detector at the frequency of peak transmission of the interference filter. In the range of frequencies and blackbody temperatures T_b of interest in these experiments,

$$B(\nu) = (2h\nu/\lambda^2) e^{-h\nu/kT_b}, \tag{12}$$

where λ is the photon wavelength and k is Boltzmann's constant. Because $h\nu/kT_b \gg 1$, one can determine the frequency at which the integrand of Eq. (11) is significant by varying T_b, as discussed in Sec. III C. Since the detector responsivity varies slowly with frequency,[22] we assume $D(\nu_i) = D(\nu_0)$. The excitation coefficient is then obtained from Eqs. (9)–(11) and is given by

$$\frac{\alpha_C}{N} = \frac{4\pi e f_b A_b \Delta\Omega_b}{S_b A L h\nu_0} \frac{\gamma}{N} \frac{S(\max)}{i} \frac{\int_0^\infty f_i(\nu) B(\nu)\, d\nu \int_V j\, dV}{\int_V \Delta\Omega j \mathcal{T}\, dV} \,, \tag{13}$$

where L is the electrode separation. In our calculations j is assumed to be independent of position. Because of the slow variation of $\mathcal{T}(\rho)$ with ρ, the results are expected to be insensitive to the distribution of j.

B. CO_2-N_2 mixtures

Measurements of the rate coefficients for the excitation of N_2 were undertaken in order to provide a test of the detector calibration and gas transmission function calculations. Nitrogen was used for this purpose, because (a) analyses of electron collisions[31, 32] in N_2 have shown that for E/N between 2×10^{-16} and 4×10^{-16} V cm^2 at least 95% of the energy gained by the electrons from the applied field is used to excite vibrational levels of N_2, and (b) the rapid collisional exchange of energy between the first excited vibrational level of N_2 (2331cm^{-1}) and the 001 level of CO_2 (2349cm^{-1}) means that with a small admixture of CO_2 the population of CO_2 in the 001 level is determined by the ratio of the readily calculated rate of vibrational excitation of N_2 to the measured decay constant 4.3-μm radiation.

The collision processes[28, 33] which need to be included in the rate equations describing the density of CO_2 molecules in the 001 level n_C and of N_2 molecules in the $v=1$ level n_N are the following:

$$CO_2(001)+N_2(0)\underset{k_{-a}}{\overset{k_a}{\rightleftharpoons}}N_2(1)+CO_2(000), \tag{14a}$$

where the number in parenthesis indicates the vibrational quantum number and[28] $k_a=(5.6\pm0.3)\times10^{-13}$ cm^3/sec at 300 K and varies as $T^{-1/2}$;

$$N_2(1)+N_2(0)\rightarrow 2N_2(0), \tag{14b}$$

where $k_b\sim10^{-17}$ cm^3/sec at 300 K and decreases rapidly as T decreases[33];

$$CO_2(001)+CO_2(000)\rightarrow CO_2(\nu_1,\nu_2)+CO_2(000), \tag{14c}$$

where ν_1 and ν_2 are indicative of the uncertainty as to the exact distribution of the energy among the ν_1 and ν_2 vibrational modes and[28] $k_c=1.1\times10^{-14}$ cm^3/sec at 300 K and 6.5×10^{-15} cm^3/sec at 200 K;

$$CO_2(001)+N_2(0)\rightarrow CO_2(\nu_1,\nu_2)+N_2(0); \tag{14d}$$

and

$$N_2(1)+CO_2(000)\rightarrow N_2(0)+CO_2(\nu_1,\nu_2)\,. \tag{14e}$$

The rate coefficients for processes (14d) and (14e) have not been separated at our temperatures, but Moore *et al.*[28] find

$$k_{de}\equiv k_d+k_ak_e/k_{-a}=3.3\times10^{-15}\ \text{cm}^3/\text{sec}$$

at 300 K. Inoue and Tsuchiya[28] find a value of 1.4×10^{-15} cm^3/sec at 200 K.

Solutions to the rate equations for the densities of vibrationally excited CO_2 and N_2, which include reactions (14a)-(14e), have been discussed by a number of authors.[28] In particular, Moore *et al.*[28] have shown that the transfer of excitation between CO_2 molecules in the 001 level n_C and N_2 molecules in the $v=1$ level n_N is fast enough so that

$$n_N/n_C=k_a[N_2]/k_{-a}[CO_2], \tag{15}$$

where $k_a/k_{-a}=e^{\Delta E/kT}$ and $\Delta E=18$ cm^{-1}. Making use of this approximation,[34] we find that the rate equation for the sum of the densities of excited CO_2 and N_2 is

$$\left(1+\frac{k_a[N_2]}{k_{-a}[CO_2]}\right)\frac{dn_C}{dt}=(k_{eN}[N_2]+k_{eC}[CO_2])n_e-n_C\{(k_b[N_2]+k_e[CO_2]+D_N/\Lambda^2)\,k_a[N_2]/k_{-a}[CO_2]+k_c[CO_2]+k_d[N_2]+gA+D_C/\Lambda^2\}. \tag{16}$$

Here we have again approximated[35] the effects of self-absorption on the escape of the 4.3-μm radiation by Holstein's g factor[26] and the effects of the diffusion of the excited molecules to the electrodes by the loss rate characteristic of the fundamental diffusion mode.[30] The normalized diffusion coefficients for the excited N_2 and CO_2 molecules, i.e., ND_N and ND_C, respectively, are expected to decrease by about a factor of 2 as the relative CO_2 concentration increases.[29] The k_{eN} and k_{eC} are the rate coefficients for excitation of the vibrational levels of N_2 and of the ν_3 mode of CO_2, respectively.

Equation (16) is very similar to Eq. (4) and yields Eqs. (6)-(8) if we replace α_C/N by

$$\frac{\alpha_M}{N}\equiv\frac{(\alpha_NX_N+\alpha_CX_C)}{N}\left(1+\frac{k_aX_N}{k_{-a}X_C}\right)^{-1} \tag{17}$$

and γ/N by

$$\frac{\gamma_M}{N}\equiv\frac{(k_bk_a/k_{-a})X_N^2+k_{de}X_CX_N+k_cX_C^2+gAX_C/N+(ND_NX_Nk_a/k_{-a}+ND_CX_C)/\Lambda^2N^2}{X_C+(k_a/k_{-a})X_N}\,. \tag{18}$$

Here $X_C=[CO_2]/N$, $X_N=[N_2]/N$, $\alpha_N/N=k_{eN}/w_e$, and $\alpha_C/N=k_{eC}/w_e$. If one neglects the radiation escape and diffusion terms in Eq. (18), the decay constant γ_M is the same as that given by Moore *et al.*[28]

For comparison with other experiments it is convenient to rewrite Eq. (18) in the form

$$\frac{\gamma'_M}{[CO_2]}\equiv\frac{\gamma_M}{[CO_2]}\left(X_C+\frac{k_a}{k_{-a}}X_N\right)-\frac{gA}{N}-\frac{(ND_NX_Nk_a/k_{-a}+ND_CX_C)}{\Lambda^2N^2X_C}$$
$$=\frac{k_bk_a}{k_{-a}}\frac{1}{X_C}+\left(k_{de}-2k_c\frac{k_a}{k_{-a}}\right)+\left(\frac{k_bk_a}{k_{-a}}+k_c-k_{de}\right)X_C\,. \tag{19}$$

Figure 4 shows a plot of $\gamma'_M/[CO_2]$ calculated using the coefficients cited in the discussion of reactions (14a)-(14e). Under the conditions of the experiments reported in this paper we find the contribution to $\gamma'_M/[CO_2]$ for the escape of radiation, i.e., gA/N, to be about 1%. The contribution of diffusion varies from about 1% at the higher total density (2×10^{17} cm^{-3}) and larger CO_2 fractions to

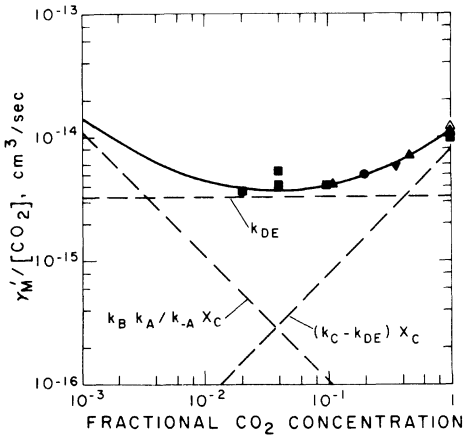

FIG. 4. Collisional destruction rate coefficient for 4.3-μm radiation in CO_2-N_2 mixture at 300 K. The solid curve is a plot of the final form of Eq. (19) evaluated using the rate coefficients cited in Sec. II B. The points show the results of various experiments with the following symbols and authors from Ref. 28: ▲: Moore *et al.*; ●: Rosser *et al.*; △: Reid, *et al.*; ▼: Inoue and Tsuchiya; and ■: the present paper. The datum of Sepucha is indistinguishable from that of Rosser *et al.* for pure CO_2.

about 10% at the lower total density (1×10^{17} cm^{-3}) and lower CO_2 concentrations.

In addition to the changes in the values of excitation and decay coefficients when N_2 is added to CO_2, one must take into account the effects of the broadening of the lines of the 4.3-μm band by nitrogen. The calculated values of the fractional transmission for two CO_2-N_2 mixtures are shown in Fig. 3. The values of τ at 300 K are seen to scale with the variable $[CO_2]\rho/[N]$ for 2% and 4% CO_2 in the mixture and for $1<\rho<4$ cm (see Appendix B). The mixture results extrapolate to values somewhat below the pure CO_2 values, because of the smaller cross sections for collisional broadening[36] of CO_2 by N_2 than by CO_2. Because of the much larger values of τ and smaller values of γ_M for the mixture than for pure CO_2, one expects a significantly improved signal-to-noise ratio for the mixtures.

III. EXPERIMENTAL APPARATUS AND PROCEDURE

A. Apparatus

The drift tube shown schematically in Fig. 2 is formed by two parallel circular disk electrodes placed inside a stainless-steel cavity. The electrodes are 4.3 cm in diameter and are 1.4 cm apart. The cathode has a concentric hole 2.5 cm in diameter in which is placed a quartz window that has been coated with a thin layer of palladium.[37] Light from a 100-W high-pressure mercury lamp mounted in a water-cooled housing passes through a 1-cm-thick uv-transmitting quartz block which absorbs the infrared portion of the spectrum. The uv light then passes through a light pipe and a sapphire window in the cavity wall to the cathode. A second sapphire window is used for viewing the radiation emitted from the gas, while a third window allows radiation from a blackbody to pass through the drift tube to the detector for calibration purposes.

The detector is a liquid-nitrogen-cooled photovoltaic indiumantimonide infrared detector[22] with a peak response near 4.5 μm. The detector output is amplified through a current-mode operational amplifier followed by an ac-coupled, $\times$1000-gain voltage amplifier. High-transparency wire screens cover the cavity exit window and the detector mount so as to shield the detector from the electric field variations which are produced as the result of modulation of the voltage across the drift tube.

The blackbody calibrating source is a blackened cone with a 0.6-cm aperture and is provided with a temperature controller capable of maintaining the cone at temperatures from 320 to 870 K to within 5 K. A chopper blade driven by a synchronous motor interrupts the output of the source at a frequency of about 65 Hz. A second aperture limits the amount of radiation falling on the detector to a value about equal to that measured during the experiment. An interference filter whose peak response is at 2345 ± 30 cm^{-1} is used to select that part of the blackbody spectrum which coincides with the $CO_2(\Delta\nu_3=1)$-band emission. This interference filter is placed at room temperature between the blackbody and the drift tube, so that it retains its measured room-temperature transmission characteristic of about 30% peak transmission and about 0.2 μm bandwidth.

The semitransparent cathode[37] is formed by vacuum deposition of an extremely thin layer of palladium on a 2.5-cm diameter ultraviolet-transmitting quartz window which had been provided with a baked-on metal contact ring. The photoelectric yield is highly dependent on the coating thickness. Although no systematic studies of photocurrent versus thickness were performed, it was found that good results are obtained with a film which is approximately 80% transmitting to room light. The maximum photocurrent obtained in vacuum is about 1 μA. In the presence of a gas the photocurrent varies roughly as $(E/N)^{1/2}$, and for values of E/N near the maxiumu used ($\sim3\times10^{-16}$ V cm^2) the photocurrent is about 2×10^{-7} A. The high-voltage pulsing unit provides a positive going, zero-based square-wave accelerating voltage of up to 1000 V to the anode of the drift

tube. It is triggered by a signal from the data collection system. The maximum voltage that can be applied without breakdown and destruction of the photocathode depends on the pressure of the gas in the drift tube and requires that $E/N < 6 \times 10^{-16}$ V cm^2. The accuracy of measurement of the peak voltage is about 1%. The electron current through the drift tube passes through a two-section, low-pass RC filter to an electrometer, and the average current is measured to an accuracy of about 5%.

The all-metal and glass gas-handling system includes a gas manifold pumped by an oil diffusion pump, a liquid-nitrogen trap, and a zeolite-trapped mechanical pump. A capacitance-type differential manometer separates the high-vacuum region from the mechanical gauge used to determine the gas density. The accuracy of the gauge is quoted as 0.2% of full scale, or 13 Pa (0.1 Torr). Bakable leak valves are used to introduce "research grade" gases into the gas manifold from high-pressure 4-MPa (40 atm) gas bottles. The manufacturers specifications are less than 0.01% and 0.001% impurity for the CO_2 and N_2, respectively. An oven was occasionally used to bake out the drift tube and gas manifold. Residual gas pressures of about 1 μPa and rates of rise of about 1 μPa/sec were obtained after bakeout.

B. Signal-averaging techniques

Two different signal-averaging techniques were used, depending upon whether the primary concern was the determination of the absolute magnitude of α_C/N or the determination of the variation of α_C/N with E/N. A discussion of both methods follows:

(1) The first method utilizes a multichannel scaler to control the experiment and collect the data for determination of the absolute value of α_C/N. The unit is programmed to switch on and off the drift tube voltage at preset channels so as to give rise to a symmetric 50% duty cycle square-wave accelerating voltage. The output of the detector-amplifier is fed into the analog-to-digital converter and is integrated for the duration of each channel. The number of sweeps performed depends on the signal-to-noise ratio of the detector output, with the maximum integration time limited by the noise generated by the analog-to-digital converter. For pure CO_2 at high E/N, integration times of about 250 sec are typical. For CO_2-N_2 mixtures, integration times of 5 sec are usually adequate. The output waveform from the multichannel signal analyzer is then recorded on punched tape and is analyzed by means of a least-squares fitting routine which determines the peak-to-peak amplitude and the time constants of the growth and decay of the detector output.

(2) The second method of running the experiment utilizes a lock-in detector to improve the signal-to-noise ratio over that obtained with the analog-to-digital converter. The reference signal output from the lock-in detector is converted into a square wave and is then used to drive the high-voltage pulsing unit. The output of the infrared detector amplifier is fed through a bandpass filter centered at the signal frequency and then into the signal channel of the lock-in detector. The output of the lock-in detector is proportional to the fundamental component of the infrared signal waveform. Careful monitoring of the signal channel was necessary so as to avoid overloading at the various stages of the lock-in amplifier. For applications at low signal-to-noise ratio, where long integration times (2000 sec) are necessary, the output of the lock-in amplifier is recorded on the multichannel scaler.

C. Calibration procedure

Calibration of the detector using the blackbody source is normally performed before and after an experimental run. The drift tube is evacuated before calibration, as any CO_2 present would attenuate the blackbody radiation. The multichannel scaler is synchronized with the chopper wheel. The peak-to-peak signal amplitude, the filter transmission data, and the calculated solid angle subtended by the detector at the blackbody aperture are used to calculate the responsivity of the detector system. A test for proper operation of the calibration system is to measure the detector output as a function of blackbody temperature as determined by an internal Pt, Pt–10%-Rh thermocouple referred to an ice bath. The detector output is observed to vary exponentially with $1/T_b$ for reference temperatures between 370 and 590 K, as expected from Eq. (12). The variation of S_b with $1/T_b$ shows that at reference temperatures below 370 K emission from the chopper blade becomes significant. Therefore a temperature of about 460 K was used for routine calibrations. The slope of an exponential plot of relative calibration signal vs $1/T_b$ showed that the detection system had a peak response at 2350 ± 100 cm^{-1}, as expected from the filter characteristics. This frequency is close enough to that of the 4.3-μm-band peak so as to justify the assumption of $D(\nu_0) = D(\nu_i)$ in Eq. (11).

D. Test for reflected signals

A test was carried out for the presence of significant signal at the detector resulting from re-

flection of the 4.3-μm radiation by the electrodes and walls of the collision chamber. For this test the detector was moved away from the cell window and an aperture was placed between the cell and the detector such that the only reflected radiation which could reach the detector was from the window on the far side of the cell. These measurements were made with the 2% CO_2 + 98% N_2 mixture, because of the high signal-to-noise ratio. When differences in geometry were taken into account, the measured excitation coefficients agreed to 5% with those obtained using a geometry which allowed the detector to view the entire collision chamber.

IV. RESULTS

A. Pure CO_2

Examples of the measured values of the peak 4.3-μm signal normalized to the current through the cell are plotted in Fig. 5 as a function of the CO_2 density for various values of E/N at 300 K. These data show that the ratio of the 4.3-μm flux reaching the detector to the electron current through the drift tube is independent of CO_2 density for densities between about 1.5×10^{17} and 7×10^{17} molecule/cm^3. At higher CO_2 densities the 4.3-μm signal per unit current is seen to decrease with increasing gas density, as expected, because of the decrease in $\mathcal{T}(\rho)$ caused by overlapping wings of the lines of the 4.3-μm bands. A decrease in the 4.3-μm signal per unit current was also observed at CO_2 densities below those shown in Fig. 5, as expected, when the loss of excited molecules increases because of diffusion to the electrodes (see Appendix A). As indicated by the square point for $X_C=1$ in Fig. 4 the decay constant for pure CO_2 at 300 K is within 10% of the accepted value. At 205 K our value is ~20% lower than the value obtained by Inoue and Tsuchiya.[28]

Figure 6 shows the excitation rate coefficients derived from data such as those of Fig. 5 when placed on an absolute scale through calibration of the detector, etc. The solid points are the averages of two absolute determinations of α_C/N at 282 and at 204 K as obtained using the multichannel analyzer to record the 4.3-μm transient from the excited CO_2 and from the calibration source. The open points were obtained at fixed gas density, e.g., 3×10^{17} molecules/cm^3, and variable electric field using the lock-in detector to determine relative values of the 4.3-μm signal. These relative values were then normalized to the absolute values for the respective gas temperatures. The α_C/N values shown in Fig. 6 were cal-

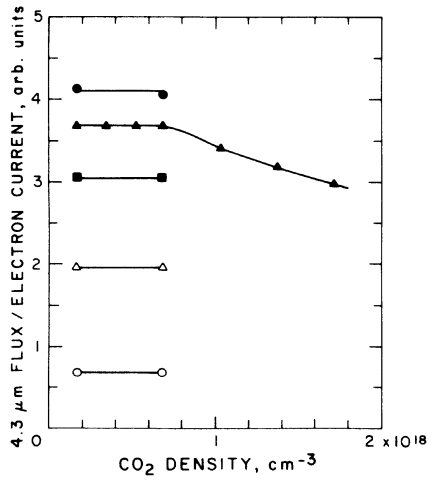

FIG. 5. Flux of the 4.3-μm radiation per unit current through excitation cell as a function of CO_2 density for various values of E/N in pure CO_2. The symbols and associated values of E/N are ●: 4.15×10^{-16}; ▲: 3.11×10^{-16}; ■: 2.07×10^{-16}; △: 1.53×10^{-16}; and ○: 1.04×10^{-16} V cm^2. The units of the ordinate are approximately 10^{-4} W/A. The lines serve only to connect points obtained at the same value of E/N.

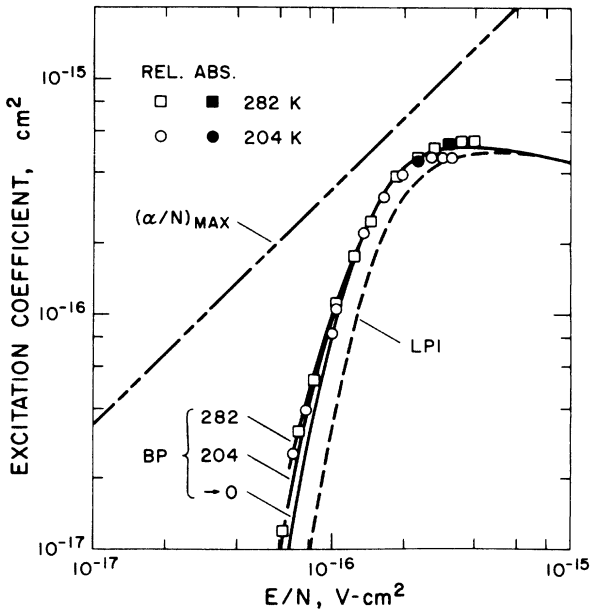

FIG. 6. Electron excitation coefficient for 4.3-μm radiation α_C/N vs E/N for pure CO_2. The ○ and ● points are relative and absolute values for 204 K, while the □ and ■ points are relative and absolute values for 282 K. The solid curves are the predictions of calculations for various gas temperatures as discussed in Sec. V, while the short dashed curve is the result of Lowke *et al.* (Ref. 19). The straight line labeled $(\alpha/N)_m$ gives the values of α_C/N which should be observed if all of the available electron energy were used to excite the ν_3 mode of CO_2.

culated using an A value[27] of 460 sec^{-1}. Note that for $E/N < 2\times10^{-16}$ V cm^2, the excitation coefficient is given empirically by $\alpha_C/N = 1.8\times10^{-15}\times\exp(-3.0\times10^{-16}N/E)$ cm^2. The data of Fig. 6 show that for $E/N > 1\times10^{-16}$ V cm^2 α_C/N is independent of the gas temperature to within the scatter of the data. Thus the ~30% increase in $\tau(\rho)$ as the temperature is increased from 204 to 282 K (see Appendix B) is accompanied by a corresponding increase in the 4.3-μm signal.

The scatter in the data points is indicative of the reproducibility of the relative values of α_C/N. The absolute values of α_C/N obtained at each gas temperature were in agreement ±10%. The manufacturer's stated accuracy for the infrared source, coupled with estimated inaccuracies in the measurement of distances, limiting aperture area, window and filter transmission, and reference temperature, lead to an estimated accuracy for the detector calibration of ±10%. Electron current measurements, fitting of the measured signal transient, evaluation of spatial integrals, and calculation of the product of $A\tau(\rho)$ are estimated to introduce an uncertainty of ±10%. Note that the uncertainty in A is partially cancelled in the product $A\tau(\rho)$, which according to the relations derived in Appendix B varies as $A^{1/2}$ under the conditiond of this experiment.

The solid curves of Fig. 6 are those calculated for pure CO_2 using the electron collision cross sections given in Sec. V while the lower dashed curve is that obtained by Lowke, Phelps, and Irwin[19] (LPI) and by Judd.[21] The rate coefficients calculated by Hake and Phelps[18] are in reasonable agreement with those of Fig. 6 at low and high E/N, but are ~25% too high for $E/N = 2\times10^{-16}$ V cm^2. The coefficients given by Nighan[20] are in good agreement with the experimental data in the region of overlapping E/N.

The straight line in Fig. 6 labeled $(\alpha/N)_m$ is obtained by dividing E/N by the energy in electron volts of the 4.3-μm photon. This line gives the values of α_C/N which would be determined from experiment if all of the electron energy were used to excite the ν_3 mode of CO_2. From the ratio of the measured values of α_C/N to $(\alpha/N)_m$ the maximum efficiency of excitation of the ν_3 mode is found to be (60 ± 10)% at $E/N = 2\times10^{-16}$ V cm^2.

B. CO_2-N_2 mixtures

The decay-constant data from our experiments in CO_2-N_2 mixtures are plotted in Fig. 4 for comparison with the smooth curve generated using Eq. (19) and the rate coefficients cited in Sec. IIB. The high values in our data may result from the accumulation of impurities in our vacuum system, which was baked only occasionally. The measurements of decay constants reported here agree sufficiently well with the data obtained by others so as to support the assumption critical to the determination of the excitation coefficients, i.e., that the number of CO_2 molecules excited to the 001 level is in equilibrium with the density of vibrationally excited N_2. The decay constants obtained at 282 and 205 K decrease with decreasing temperature approximately as expected.[28] The experimental excitation coefficients $(\alpha_N X_N + \alpha_C X_C)/N$ for a mixture of 2% CO_2 and 98% N_2 are shown as points in Fig. 7. The excitation coefficients are calculated using Eq. (17) and Eq. (13) as modified by replacing α_C/N by α_M/N and γ/N by γ_M/N. Because of the much larger signal-to-noise ratio observed in the CO_2-N_2 mixtures, all of the data were obtained with the multichannel scaler and each point shown is an absolute determination. The estimated uncertainties in the values of $(\alpha_N X_N + \alpha_C X_C)N$ are the same as for pure CO_2. The measurements shown were made at total gas densities of $(1-2)\times10^{18}$ cm^{-3} so as to allow with an estimated accuracy of ± 10% the measurement of the change in pressure caused

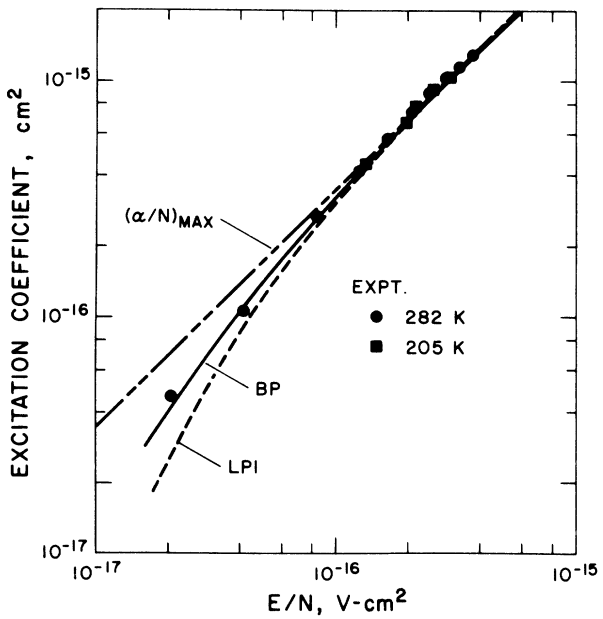

FIG. 7. Electron excitation coefficient for vibrational levels of N_2 and 001 level of CO_2 $(\alpha_N x_N + \alpha_C x_C)/N$ vs E/N for 2% N_2 in CO_2. The ● and ■ points were obtained at 282 and 205 K, respectively. The solid curve is that predicted using the cross-section set discussed in Sec. V, while the short dashed curve is the result of calculations by Lowke *et al.* (Ref. 19). The straight line gives the excitation coefficient expected if all of the electron energy were used to excite vibrational levels of N_2 and the ν_3 mode of CO_2.

by the addition of CO_2. Although the measured decay constants shown in Fig. 4 are sometimes significantly larger than expected for the CO_2-N_2 mixture, the scatter in the excitation coefficients shown in Fig. 7 is small. For E/N greater than 1.5×10^{-16} the experimental coefficients lie on the $(\alpha/N)_m$ line to well within the estimated uncertainty of the data of ±15%.

The solid curves of Fig. 7 show the $(\alpha_N X_N + \alpha_C X_C)/N$ values calculated for 2% CO_2 + 98% N_2 using the electron collision cross sections given in Sec. V. For E/N between 2×10^{-16} and 4×10^{-16} V cm^2 these calculations show that 90%–95% of the electron energy is used to excite the vibrational states of N_2 via the large resonance[10] centered at 2.2 eV and from 5%–1% of the electron energy is used to excite the ν_3 mode of CO_2. Thus the predicted efficiency of electron excitation of states capable of supplying energy for emission at 4.3 μm is 95% or larger for the higher E/N. Furthermore, the 5% or less inefficiency is partially canceled by the energy transferred from thermal motion to vibration as the N_2 molecule vibrationally relaxes and transfers the vibrational excitation to the CO_2. Because of this high net excitation efficiency and because of the simple relation between $(\alpha/N)_m$ and E/N, there is very little uncertainty (± 5%) in the predicted values of $(\alpha_N X_N + \alpha_C X_C)/N$ for E/N greater than 1.5×10^{-16} V cm^2. The agreement between the predicted and experimentally determined excitation coefficients is therefore considered to be a verification of the calibration of the detection system for measurement of 4.3-μm radiation and of the calculation of $A\mathcal{T}(\rho)$.

At E/N below 10^{-16} V cm^2 the experimental values of $(\alpha_N X_N + \alpha_C X_C)/N$ lie well above the values predicted using the cross sections of LPI.[19] In this range of E/N the principal contribution to the excitation coefficient is from $\alpha_C X_C/N$, i.e., at $E/N = 2\times10^{-17}$ V cm^2 the ratio $\alpha_C X_C/\alpha_N X_N$ is 9.

V. VIBRATIONAL EXCITATION CROSS SECTIONS

The set of vibrational excitation cross sections for CO_2 used to calculate the solid curves of Figs. 6 and 7 is shown in Fig. 8. As in earlier determinations[18,19] of cross-section sets, the weighted sum of the vibrational excitation cross sections is determined primarily by fitting calculated and experimental plots of the energy exchange collision frequency versus characteristic energy[18] ϵ_K for pure CO_2. Similarly, in the present analysis, the cross section for excitation of the ν_3 mode, which is labeled Q_{001} in Fig. 8, is determined primarily by fitting calculated and experimental plots of k_{001} vs ϵ_K for CO_2. Here, the experimental values of k_{001} are calculated from

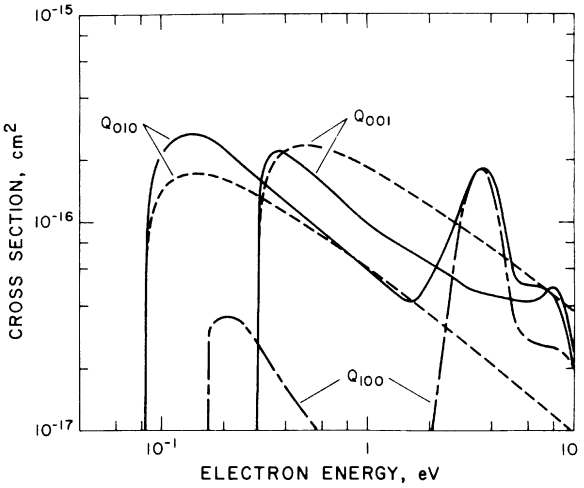

FIG. 8. Cross sections for excitation of lowest vibrational levels of bending (010), symmetric stretch (100), and asymmetric stretch (001) modes of CO_2. The solid curves are derived from analysis of this experiment, as discussed in the text. The short dashed curves are calculated from the transition probabilities of Penner and Olfe (Ref. 27) and the Born approximation formulas of Takayanagi (Ref. 16).

the α_C/N values of Fig. 6 and earlier measurements[18] of w and are plotted against previously measured ϵ_K values.[18] Note that this approach could not be used for data obtained at $E/N > 2.1\times10^{-16}$ V cm^2, because of the absence of experimental electron drift velocity data. We have therefore used the cross-section data of Andrick *et al.*[12] without change for electron energies above 1.5 eV. Note that at $E/N < 10^{-16}$ V cm^2 the solid curve calculated without allowance for heating of electrons in deexcitation collisions with thermally excited vibrational modes, i.e., the $T \to 0$ curve, lies significantly below the curves in which an approximate accounting was made of deexcitation processes.[38] The sensitivity of the k_{001} vs ϵ_K plot to the magnitude of the assumed cross section is ±10%. We therefore estimate that the accuracy of the derived cross section for excitation of the ν_3 mode is ±20%.

The cross section for excitation of the ν_3 mode obtained from this analysis is compared with the predictions of the Born approximation[16] in Fig. 8. The derived cross section increases slightly more rapidly than the Born approximation near threshold and at energies above 0.4 eV is significantly smaller than that calculated using the Born approximation and the transition probability used in Sec. IV. The derived cross section for the 001 level differs significantly from that of Boness and Schulz.[11] The curves of Fig. 8 show that it is possible to find cross sections

for excitation of the 010 and 100 levels which are consistent with the electron transport data,[18] the α_C/N data of Figs. 6 and 7, the threshold excitation data of Stamatovic and Schulz,[39] and the cross-section data of Andrick *et al.*[12] Unfortunately, these data do not place much in the way of constraints on the cross section for excitation of the 100 level at energies between 0.2 and 1.5 eV.

VI. SUMMARY

The electron-drift-tube technique has been used to measure the rate coefficients for electron excitation of molecules with long radiative lifetimes, i.e., for the excitation of CO_2 molecules to the 001 and 011 levels. This is accomplished through the use of relatively high gas densities so as to reduce the loss of excited molecules to the walls and to increase the number of collisions of electrons with the gas molecules. Extension of the technique to molecular states with even longer radiative lifetimes seems feasible, provided that the molecules emit at wavelengths where suitable detectors are available.

The measured rate coefficients for excitation of the asymmetric stretch mode of CO_2 agree reasonably well with earlier predictions at the higher values of E/N. However, at low E/N the measured rate coefficients are much larger than predicted and suggest that previous work has overestimated the cross sections for excitation of the bending and symmetric stretch modes of CO_2 at low electron energies. The new set of vibrational excitation cross sections proposed in this paper is consistent with most published data, but needs to be tested against measurements of the division of the excitation energy among the bending and symmetric stretch modes of CO_2.

ACKNOWLEDGMENTS

The authors are especially indebted to R. S. Cohen, who obtained measurable signals with the apparatus while he and one of the authors (AVP) were at Westinghouse Research Laboratories. They also indebted to F. Wible and H. Gartska for assistance in the design and construction of the experimental tube and to the management of Westinghouse Research Laboratories for the gift of the experimental tube. The authors wish to acknowledge the help of S. A. Lawton in obtaining some of the data and helpful discussions of CO_2 cross-section data with G. J. Schulz.

APPENDIX A: EFFICIENCY OF PHOTON PRODUCTION

The purpose of this appendix is to present a description of the variation with CO_2 density of the ratio the number of photons emitted from the CO_2-filled drift tube to the number of electrons passing through the CO_2, i.e., of the efficiency of the experiment for 4.3-μm photon production. Such an analysis serves to demonstrate the increase in photon signal which results from operation of the collision chamber at high gas densities and to delineate the range of gas densities over which one expects to obtain the density-independent signal discussed in Sec. II A. In this appendix we will simplify the discussion by considering only steady-state conditions and the limiting forms for the excitation efficiency versus density and so will not consider the complex density dependence in the transition regions. For the purposes of this calculation the electrons are assumed to be injected into the tube with 1 eV energy. The electron field applied to the gap is assumed to be given by $E = 3 \times 10^{-16} N$ V/cm, i.e., a field which produces negligible electron acceleration at low gas densities and $E/N = 3 \times 10^{-16}$ V cm^2 at high gas densities. This E/N value is near the maximum used in our experiment and results in a relatively large rate coefficient for excitation of the CO_2 molecules to the 001 state.

The predicted efficiency of 4.3-μm photon production is shown in Fig. 9 for a range of CO_2 densities from 10^{13} to 10^{19} cm^{-3}. For CO_2 densities below 3×10^{14} cm^{-3}, i.e., region 1 of the curve of Fig. 9, the photon production efficiency is equal to the product of the fraction of the electrons which excite CO_2 molecules to the 001 vibrational state, $Q_C NL = 10^{-16} N \times 1.4$, and the fraction of the excited

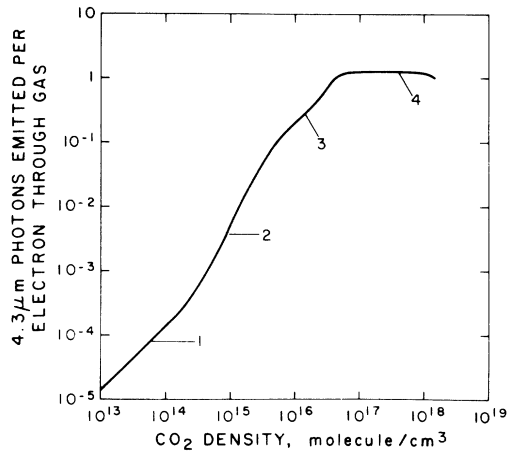

FIG. 9. Density dependence of the efficiency of production of 4.3-μm photons in pure CO_2. This calculation is for a collision chamber 1.4 cm long, photoelectrons with an initial energy of 1 eV, and a gas temperature of 300 K. See Appendix A for a discussion of the processes of importance in sections of the curve labeled 1–4. Regions 2 and 3 and the curved portions are only approximate representations of the true curve.

molecules which radiate before striking the electrodes, i.e., roughly $AL(2\langle v_m\rangle)^{-1} = 0.01$. Here $Q_C = 10^{-16}$ cm^2 and $\langle v_m\rangle$ is the average speed of the CO_2 molecule.

In the CO_2 density range from about 10^{14} to about 10^{15} cm^{-3} the mean free paths for excited CO_2 molecules, for electrons and for 4.3-μm photons, become comparable with the electrode separation of 1.4 cm. Thus in the gas density range from 3×10^{14} to 3×10^{16} cm^{-3} the fraction of CO_2 molecules in the 001 state which radiate is approximately $AL^2N^2(\pi^2D_mN)^{-1} \approx 5\times10^{-17}N$, where D_m is the diffusion coefficient for CO_2 molecules in the 001 state and where we have approximated the spatial distribution of excited molecules by that for the fundamental diffusion mode between completely absorbing electrodes.[29] For gas densities between 3×10^{14} and 10^{16} the fractional transmission of the 4.3-μm radiation is controlled by the Doppler-broadened portion of the spectral lines and is given approximately by $11\times10^{14}/N\rho$, where ρ is the average distance from the excited molecules to the window of the excitation cell (see Appendix B). Finally, as a result of the multiple collisions at CO_2 densities between about 10^{15} and about 3×10^{15} cm^{-3} the effective number of excitation collisions[40] for 1-eV electrons is increased by $1.5Q_mNL \approx 1.2\times10^{-15}N$. Here Q_m is the cross section for momentum transfer collisions.[19] The product of the last two effects is nearly unity, so that the net excitation efficiency remains approximately $5\times10^{-33}N^2$ throughout region 2 of the curve of Fig. 9.

At CO_2 densities of about 3×10^{15} cm^{-3} the applied voltage becomes comparable with the initial electron energy, and for densities significantly above 4×10^{16} cm^{-3} the electrons reach a steady-state distribution of electron energies in a distance short compared to the electrode separation. The number of excited molecules produced per electron crossing the tube is then given by $\alpha_C NL \approx 7\times10^{-16}N$ for $E/N = 3\times10^{-16}$ V cm^2. For CO_2 densities up to about 3×10^{16} cm^{-3} the loss of excited molecules is still by diffusion and the fraction of molecules which radiate in the 4.3-μm band remains $4.4\times10^{-17}N$. Similarly, the fractional transmission is Doppler controlled for densities up to about 2×10^{16} cm^{-3}. The net photon production efficiency is therefore approximately $2\times10^{-17}N$ for CO_2 densities between 3×10^{15} and about 2×10^{16} cm^{-3}, i.e., region 3 of the curve of Fig. 9.

At CO_2 densities above 2×10^{16} cm^{-3} the transmission of the 4.3-μm radiation is determined by by the collision-broadened portion of the spectral lines, and at densities above about 3×10^{16} cm^{-3} collisional quenching dominates over loss by diffusion. Using the quenching coefficient for pure CO_2 discussed in Sec. II B, the fraction of the excited molecules which emit 4.3-μm-band radiation is $4.5\times10^{16}/N$, while according to Appendix B the fractional transmission of the 4.3-μm bands is about 0.04. These results, coupled with the electron excitation coefficient, yield a net photon production efficiency of approximately unity. This result is valid for CO_2 densities between about 3×10^{16} and about 10^{18} cm^{-3}, i.e., region 4 of the curve of Fig. 9. At higher CO_2 densities the absorption profile of the various lines of the 4.3-μm bands begin to overlap and the fraction of the radiation reaching the detector decreases with increasing CO_2 density.

The calculations of photon production efficiency shown in Fig. 9 illustrate the large, i.e., more than three orders of magnitude, increase in radiated signal which results from operation of the collision chambers at high CO_2 densities. While one can obtain relatively large electron currents, e.g., 10^{-6} A at 1 eV and at the low gas densities characteristic of electron beam operation, the fractional energy resolution attainable at the higher beam currents and lower electron energies is not much better than that obtained at the lower E/N of the present drift-tube experiments, and the radiated signal is much smaller.

An evaluation of the utility of the drift-tube technique requires some discussion of the useful and available current levels. In order to limit the space charge induced distortion of the electric field[41] to less than 10%, the currents in the drift tube should be less than about 2×10^{-7} A/cm^2 at $E/N = 7\times10^{-17}$ V cm^2 and 3×10^{-6} A/cm^2 at $E/N = 3\times10^{-16}$ V cm^2. At higher E/N the formation of low-mobility negative ions will limit the usable current further. For example, if 3% of the electrons form negative ions while crossing the drift tube, space-charge-free operation requires roughly an order-of-magnitude reduction in the total current from values allowed in the absence of attachment. The maximum current densities which we have obtained with gas in the drift tube are about 2×10^{-7} A/cm^2 at the higher E/N. Presumably, means can be found to activate the photocathodes or increase the uv intensity so as to approach the limits set by space charge.

The drift-tube technique presented in this paper complements the various electron scattering experiments[10–12] by providing excitation data of relatively high accuracy for those excited states which radiate at wavelengths for which good detectors are available. The drift-tube results include the effects of the cascade of excitation from higher levels and of excitation transfer from other excited states, whereas the electron scattering experiments measure only the effects of the initial collision of the electron with the molecule.

APPENDIX B: TRANSMISSION OF 4.3-μm RADIATION

In this appendix the theory and numerical results of calculations of the fractional transmission of the 4.3-μm band are presented. In addition, approximate formulas for the fractional transmission are derived which show the scaling parameters appropriate to various ranges of gas density and distance. Although related radiation transport problems have been considered by several authors,[26,42,43] none of their results are directly applicable to the experiments analyzed in this paper.

The fractional transmission $\mathcal{T}(\rho,N)$ is defined by

$$\mathcal{T}(\rho,N)=\frac{\int_0^\infty R_\omega(N)e^{-\rho k_\omega(N)}\,d\omega}{\int_0^\infty R_\omega(N)\,d\omega}, \tag{B1}$$

where $R_\omega(N)$ is the total energy emitted in the wave-number interval $d\omega$ per unit solid angle in $\Delta\nu_3=1$ transitions, k_ω is the absorption coefficient at ω, and ρ is the distance from the point of emission to the point of observation. Both R_ω and k_ω are sums of the contributions of a large number of lines corresponding to the various rotational and vibrational transitions of the several isotopic forms of the CO_2 molecule. Thus

$$R_\omega=a(\omega)\sum_{v',J'} n(v')\Omega_J p_J \phi(\Delta\omega_J), \tag{B2}$$

$$k_\omega=\sigma(\omega)\sum_{v,J} n(v)\Omega_J p_J \phi(\Delta\omega_J). \tag{B3}$$

Here $a=\frac{16}{3}\pi^3 c\omega^4\beta^2$, $\sigma=\frac{8}{3}(\pi^3/hc)\omega\beta^2$, β^2 is the radial portion of the dipole matrix element for the $\Delta\nu_3=1$ transitions, p_J is the fraction of the CO_2 molecules in the Jth rotational state at the gas temperature,[27] Ω_J is the J-dependent portion of the dipole matrix element,[27] $\phi(\Delta\omega)$ is the normalized spectral line shape for a particular vibronic transition, $n(v')$ and $n(v)$ are the densities of the excited and ground vibrational states of the transition, c is the speed of light, h is Plank's constant, and $\Delta\omega_J=\omega-\omega_J$ is the wave-number separation from the center of the line at ω_J. β^2 is obtained from the integrated band intensity α using[27]

$$\beta^2=\frac{3hc}{8\pi^3\omega}\frac{\alpha}{N}=\frac{3hA}{64\pi^4\omega^3},$$

where N is the number of molecules per unit volume under the conditions of the measurement of α. The sum in Eq. (B2) is over the upper rotational and vibrational states v' and J', while the sum in Eq. (B3) is over the lower states v and J.

The spectral line shapes used in these calculations are assumed to be Lorentzian, i.e.,

$$\phi(\omega)=\frac{b_J/\pi}{b_J^2+\Delta\omega_J^2}. \tag{B4}$$

The line-broadening parameters vary with temperature and rotational quantum number and were taken from Yamamoto, Tanaka, and Aoki[36] for broadening by CO_2 and by N_2. The positions of the line centers were calculated from the constants given by Cihla and Chedin.[44] The integrated band intensity was assumed to be 1.10×10^{-16} molecule^{-1} cm^2 cm^{-1} from Penner and Olfe.[27] Vibrational transitions included in the calculation were the $001\rightarrow000$ and $011\rightarrow010$ bands of $^{12}C\,^{16}O_2$ and the $001\rightarrow000$ band of $^{13}C\,^{16}O_2$. The relative populations of the states of the bending mode, i.e., of [010]/[000] and of [011]/[001], were assumed to be determined by the gas temperature, while the populations of the corresponding states of the $^{13}CO_2$ and $^{12}CO_2$ molecules were assumed to be given by the natrual ^{13}C to ^{12}C abundance ratio, i.e., 1.1%. The calculations for pure CO_2 were tested by comparing the computed spectral absorptance of white light with the measurements of Burch and Gryvnak.[45] The agreement of the integrated absorption is better than 10%.

The calculated values of fractional transmission are shown in Fig. 3. Here $\mathcal{T}(N,\rho)$ is plotted against $([CO_2]/N)\rho$ so as to emphasize the approximate $\rho^{-1/2}$ dependence and the dependence on $[CO_2]/N$, e.g., the lack of dependence on $[CO_2]$ in pure CO_2 at these CO_2 densities. The calculated points for 205 K are (75 ± 5)% of the values shown for 300 K. The difference is largely explained by the absence of the $011\rightarrow010$ or "hot band" radiation at the lower temperature. Because of computer costs, calculations were made at only a few gas densities. The only other calculations with which we have been able to compare are those of Margottin-Maclou, Doyennette, and Henry.[26] Values of $\mathcal{T}(\rho)$ obtained from their decay constants are somewhat higher than our values.

Approximate expressions for $\mathcal{T}(\rho)$ can be obtained by assuming that each emission line of the 4.3-μm band is absorbed only by its inverse transition, i.e., that the lines of the band do not overlap significantly. This assumption allows one to ignore the summation in Eq. (B3) and to carry out the integration in Eq. (B1) on a line-by-line basis. Thus

$$\mathcal{T}(\rho,N)=\sum_{v',J'}\frac{n(v')}{n_C}p_J\mathcal{T}_J(\rho,N), \tag{B5}$$

where

$$\mathcal{T}_J(\rho,N)=\int_0^\infty \phi(\Delta\omega_J)\exp[-\rho k_p(J)\phi(\Delta\omega_J)]\,d\omega$$

and $n(v')/n_C$ is the fraction of the vibrationally excited CO_2 in the vth vibrational state. If we neglect

the variation of b_j with J in Eq. (B4), as is approximately true for large J, then for high densities

$$\mathcal{T}_J(\rho) = [\pi k_p(J)\rho]^{-1/2},$$

where for large J and both the P and R branches

$$k_p(J) = (k_0/Q_R Q_V) J \exp(-BJ^2/kT),$$

$k_0 = \lambda^2 AN/8\pi^2 cb$, $Q_R = kT/2B$, and Q_V is the vibrational partition function.[27] Here k_0 is the absorption coefficient expected at line center if all of the lines of the band coincided.

Since we have assumed J large, the sum in Eq. (B5) can be approximated by an integral, so that

$$\mathcal{T}(\rho) = \Gamma(\tfrac{3}{4})(2Q_V)^{1/2}(Q_R)^{1/4}(\pi k_0 \rho)^{-1/2}. \quad \text{(B6)}$$

Using $b = 3.5 \times 10^{-21} N$ cm^{-1}, $k_0 = 9240$ cm^{-1}, and neglecting hot bands and isotope effects, we find that Eq. (B6) yields $\mathcal{T}(\rho) = 0.041/\rho^{1/2}$ at 300 K, compared to $0.047/\rho^{1/2}$ calculated with the line-by-line evaluation of $\mathcal{T}(N,\rho)$. When the values of $\mathcal{T}(\rho)$ for the $011 \rightarrow 010$ hot band and the $^{13}C\,^{16}O_2$ band are evaluated using the appropriately adjusted coefficients in Eq. (B6) and their contributions included in Eq. (B5), the result is $\mathcal{T}(\rho) = 0.054\rho^{1/2}$, compared to $0.060/\rho^{1/2}$ calculated with the line-by-line evaluation of $\mathcal{T}(\rho)$. Note that the relatively large change (~30%) in $\mathcal{T}$ attributed to $011 \rightarrow 010$ radiation occurs in spite of the small ratio of 011 and 001 populations (~8%) at 300 K.

The application of this same approach to CO_2-N_2 mixtures in the limit of small $[CO_2]/[N_2]$ yields

$$\mathcal{T}(\rho) = \frac{\Gamma(\frac{3}{4})(2Q_V)^{1/2}(Q_R)^{1/4}}{(\pi k_0)^{1/2}} \times \left(\frac{k(N_2)}{k(CO_2)}\right)^{1/2} \left(\frac{[CO_2]}{[N_2]}\rho\right)^{-1/2}. \quad \text{(B7)}$$

Here $k(N_2)$ and $k(CO_2)$ are average rate coefficients for collisional broadening of the 001 levels by N_2 and CO_2, e.g., $k(CO_2) = b/[CO_2]$. Equation (B7) shows that $\mathcal{T}(\rho)$ is expected to be a function only of $[CO_2]\rho/N$ when collision broadening dominates the line profiles and the $[CO_2]/[N_2]$ ratio is small. These conditions appear to be rather well satisfied for the line-by-line calculations for mixtures shown in Fig. 3. Note, however, the departure from the square-root dependence at low values of $[CO_2]\rho/N$ caused by the approach to optical transparency.

At densities below about 10^{16} cm^{-3} in pure CO_2 the important portions of the line profiles for our experiments are governed by Doppler broadening. A derivation for nonoverlapping Doppler-broadened lines similar to the preceding calculation for collision-broadened lines has been carried out by Kumer and James.[43] For the purposes of Appendix A it is sufficient to note that their results for 225 K and $[CO_2]\rho > 3 \times 10^{15}$ cm^2 can be approximated by $\mathcal{T}(N,\rho) = 8 \times 10^{14}([CO_2]\rho)^{-1}$. For Doppler broadening we expect $\mathcal{T}(N,\rho)$ to vary approximately as T.

---

*Work supported in part by the Defense Nuclear Agency through the Air Force Cambridge Research Laboratories.

† Present address: University of Jordan, Amman, Jordan.

‡ Staff Member, Laboratory Astrophysics Division, National Bureau of Standards, and Professor Adjoint, Department of Physics and Astrophysics, University of Colorado.

[1] For recent reviews of electron-drift-tube experiment and theory, see A. Gilardini, *Low Energy Collisions in Gases* (Wiley, New York, 1972), Chaps. 3 and 4; and L. G. H. Huxley and R. W. Crompton, *The Diffusion and Drift of Electrons in Gases* (Wiley, New York, 1974), Chap. 12.

[2] S. J. B. Corrigan and A. V. Engel, Proc. R. Soc. A245, 335 (1958).

[3] W. Legler, Z. Phys. 173, 169 (1963).

[4] K. J. Nygaard, J. Appl. Phys. 36, 743 (1965).

[5] Rate coefficients for dissociation of CO_2 were measured by K. K. Corvin and S. J. B. Corrigan, J. Chem. Phys. 50, 1570 (1969). For a review of rate coefficients appropriate to molecular dissociation in electrical discharges, see F. Kaufman, Adv. Chem. Ser. 80, 29 (1969).

[6] M. J. Druyvesteyn and F. M. Penning, Rev. Mod. Phys. 12, 87 (1940).

[7] A. V. Phelps, Rev. Mod. Phys. 40, 399 (1968).

[8] A. J. Demaria, Proc. IEEE 61, 731 (1973).

[9] M. Shimizu and O. Ashihara, Publ. Astron. Soc. Jpn. 24, 201 (1972).

[10] For a review of measurements and interpretation of vibrational excitation of molecules, see G. J. Schulz, Rev. Mod. Phys. 45, 423 (1973), and in *Principles of Laser Plasmas*, edited by G. Bekefi (Wiley, New York, 1976).

[11] M. J. W. Boness and G. J. Schulz, Phys. Rev. Lett. 21, 1031 (1968); D. Spence, J. L. Mauer, and G. J. Schulz, J. Chem. Phys. 57, 5516 (1972); M. J. W. Boness and G. J. Schulz, Phys. Rev. A 9, 1969 (1974).

[12] A. Andrick, D. Danner, and H. Ehrhardt, Phys. Lett. 29A, 346 (1969); D. Danner, Ph.D. thesis (Universitat Trier-Kaiserslauten, Germany, 1970) (unpublished).

[13] E. R. Murray, C. H. Kruger and M. Mitchner, J. Chem. Phys. 62, 388 (1975). In our opinion the conclusions regarding vibrational excitation cross sections in this paper are questionable, because the electrostatic probe measurements at the high pressures of these experiments lead to electron "temperatures" which are much too high. See P. Bletzinger and A. Garscadden, Proc. IEEE 59, 675 (1971).

[14] A. S. Biryukov, B. F. Bordietz, and L. A. Shelepin,

in *Proceedings of the Ninth International Conference on the Phenomena in Ionized Gases, Bucharest, 1969*, edited by G. Musa, I. Ghica, A. Popesev, and L. Năstase (Academiei Republicii Socialiste Roumania, Bucharest, 1969), p. 34.

[15]M. C. Gower and A. I. Carswell, J. Appl. Phys. 45, 3922 (1974). The rate coefficients for the deexcitation of vibrationally excited CO_2 cited in this reference are about two orders of magnitude larger than values calculated using the cross section of Refs. 18–20 or of Sec. V. Relative excitation efficiencies were obtained by D. R. Shure, P. D. Coleman, and T. A. deTemple, J. Appl. Phys. 44, 2923 (1973).

[16]K. Takayanagi, J. Phys. Soc. Jpn. 21, 507 (1966); Y. Itikawa, Phys. Rev. A 3, 831 (1971).

[17]T. Sawada, D. J. Strickland and A. E. S. Green, J. Geophys. Res. 77, 4812 (1972).

[18]R. D. Hake and A. V. Phelps, Phys. Rev. 158, 70 (1967).

[19]J. J. Lowke, A. V. Phelps, and B. W. Irwin, J. Appl. Phys. 44, 4664 (1973).

[20]W. L. Nighan, Phys. Rev. A 2, 1989 (1970).

[21]H. Gündel, Beitr. Plasma Phys. 12, 159 (1972); W. P. Allis and H. A. Haus, J. Appl. Phys. 45, 781 (1974); C. B. Mills, *ibid.* 45, 1336 (1974); A. N. Lobanov and A. F. Suchkov, Kvant. Elektron. 1, 1527 (1974) [Sov. J. Quantum Electron. 4, 843 (1975)]; O. P. Judd, J. Appl. Phys. 45, 4572 (1974).

[22]According to manufacturer's specifications the relative response is a maximum at 4.3 μm and decreases to 90% at 3.6 and 4.9 μm and to 50% at 2.2 and 5.4 μm.

[23]The maximum energy input per molecule in our pure-CO_2 experiments is about 2×10^{-4} eV and produces an increase in the vibrational temperature of the ν_3 mode of less than 0.3 K.

[24]L. O. Hocker, M. Kovacs, C. K. Rhodes, G. W. Flynn, and A. Javan, Phys. Rev. Lett. 17, 233 (1966).

[25]I. Burak, Y. Noter and A. Szöke, IEEE J. Quantum Electron QE-9, 541 (1973); L. Doyennette, M. Margottin-Maclou, A. Chakroun, H. Gueguen, and L. Henry, J. Chem. Phys. 62, 440 (1975).

[26]T. Holstein, Phys. Rev. 83, 1159 (1951); M. Margottin-Maclou, L. Doyennette, and L. Henry, Appl. Opt. 10, 1768 (1971).

[27]S. S. Penner and D. B. Olfe, *Radiation and Reentry* (Academic, New York, 1968), p. 261. Note that the interpretation of the data given in this reference and the present paper is different from that of many other papers in that we assume that the measured integrated intensities are for a density appropriate to 1 atm at the temperature of the measurement (297 K).

[28]C. B. Moore, R. E. Wood, B.-L. Hu, and J. T. Yardley, J. Chem. Phys. 46, 4222 (1967); W. A. Rosser, Jr., A. D. Wood, and E. T. Gerry, *ibid.* 50, 4996 (1969); J. Reid, B. K. Garside, and E. A. Ballik, IEEE J. Quantum Electron. QE-9, 602 (1973); A. S. Biryukov, V. K. Konyukhov, A. I. Likovnikov, and R. I. Serikov; Zh. Eksp. Teor. Fiz. 66, 1248 (1974) [Sov. Phys.-JETP 39, 610 (1974)]; R. C. Sepucha, Chem. Phys. Lett. 31, 75 (1975); G. Inoue and S. Tsuchiya, J. Phys. Soc. Jpn. 38, 870 (1975); 39, 479 (1975). We have not compared our results with the results of optical-acoustic measurements because of the differences in interpretation of the characteristic times.

[29]M. Kovacs, D. Ranachandra Rao, and A. Javan, J. Chem. Phys. 48, 3339 (1968); L. Doyennette, M. Margottin-Maclou, H. Gueguen, A. Carion, and L. Henry, *ibid.* 60, 697 (1974).

[30]A. V. Phelps and A. O. McCoubrey, Phys. Rev. 118, 1561 (1960).

[31]A. G. Engelhardt, A. V. Phelps, and C. G. Risk, Phys. Rev. 135, A1566 (1964).

[32]The estimate of 95% is based on a calculation of the energy loss to rotational excitation using the theoretical cross sections of P. G. Burke and A.-L. Sinfailam, J. Phys. B 3, 641 (1971), and P. G. Burke and N. Chandra, *ibid.* 5, 1696 (1972). The fraction of the electron energy lost to rotational excitation in the analysis of Ref. 31 was considerably less than 5% in the range of E/N cited.

[33]R. L. Taylor and S. Bitterman, Rev. Mod. Phys. 41, 26 (1966).

[34]An approximate expression for the larger decay constant for the full set of equations for CO_2–N_2 mixtures is $k_a[N_2]+k_{-a}[CO_2]$ (see Ref. 28). For conditions appropriate to our experiments, the ratio of the decay constants is greater than 50:1.

[35]It should be noted that the "fundamental mode" diffusion and radiation corrections tend to underestimate the true corrections through their failure to account for the more rapid decay of excited molecules produced near the electrode boundaries. On the other hand, the use of the fundamental diffusion mode solution tends to overestimate the loss of excited molecules to the electrodes by neglecting the possibility of reflection of vibrationally excited molecules (see Ref. 29).

[36]G. Yamamoto, M. Tanaka, and T. Aoki, J. Quant. Spectrosc. Radiat. Transfer 9, 371 (1969); J.-P. Bouanich and C. Brodbeck, *ibid.* 14, 141 (1974).

[37]J. L. Moruzzi, Rev. Sci. Instrum. 38, 1284 (1967).

[38]Since our technique for solution of the Boltzmann equation does not include discreet electron energy increases caused by deexcitation collisions, the effects of these collisions have been approximated by replacing the cross sections for excitation of the 010 and 100 levels by a fictitious rotational excitation process, such that the energy exchange collision frequency agreed with experiment (see Refs. 18 and 19). The validity of this approximation needs to be tested using the final cross-section set of Fig. 8 and the complete Boltzmann equation.

[39]A. Stamatovic and G. J. Schulz, Phys. Rev. 188, 213 (1969).

[40]P. J. Chantry, A. V. Phelps, and G. J. Schulz, Phys. Rev. 152, 81 (1966).

[41]J. D. Cobine, *Gaseous Conductors* (Dover, New York, 1958), p. 128.

[42]L. Doyennette, Ann. Phys. (Paris) 253 (1969).

[43]J. B. Kumer and T. C. James, J. Geophys. Res. 79, 638 (1974).

[44]Z. Cihla and A. Chedin, J. Mol. Spectrosc. 40, 337 (1971).

[45]D. E. Burch and D. A. Gryvnak, J. Quant. Spectrosc. Radiat. Transfer 6, 229 (1966); see their Fig. 11.